Ab Initio, Transition State Theory, and Kinetic Modeling Study of the HO2-Assisted Keto–Enol Tautomerism Propen-2-ol + HO2 # Acetone + HO2 under Combustion, Atmospheric, and Interstellar Conditions

Ab Initio, Transition State Theory, and Kinetic Modelling Study of the HO_2-assisted Keto–enol Tautomerism Propen-2-ol + HO_2 ⇔ Acetone + HO_2 Under Combustion, Atmospheric, and Interstellar Conditions

M. Monge-Palacios, [a*] E. Grajales-González [a] and S. Mani Sarathy[a]

[a]King Abdullah University of Science and Technology (KAUST), Clean Combustion Research Center (CCRC), Physical Science and Engineering (PSE), Thuwal 23955-6900, Saudi Arabia.

ABSTRACT: Keto–enol tautomerisms are important reactions in gaseous and liquid systems with implications in different chemical environments, but their kinetics have not been widely investigated. These reactions can proceed via a unimolecular process or may be catalyzed by another molecule. This work presents a theoretical study of the HO_2-catalyzed tautomerism that converts propen-2-ol into acetone at conditions relevant to combustion, atmospheric and interstellar chemistry. We performed CCSD(T)/aug-cc-pVTZ//M06-2X/cc-pVTZ *ab initio* and multi-structural torsional variational transition state theory calculations to compute the forward and reverse rate constants. These rate constants have not been investigated previously, and modellers approximate the kinetics by comparison to analogue reactions. Two features of the potential energy surface of the studied tautomerism are highlighted. First, the HO_2 radical exhibits a pronounced catalytic effect by inducing a double hydrogen atom transfer reaction with a much lower barrier than that of the unimolecular process. Second, a pre-reactive complex is formed with a strong OH···π hydrogen bond. The role of the studied reaction under combustion conditions has been assessed via chemical kinetic modelling of 2-butanol (a potential alternative fuel) oxidation. The HO_2-assisted process was found to not be competitive with the unimolecular and HCOOH-assisted tautomerisms. The rate constants for the formation of the pre-reactive complex were calculated with the variable reaction coordinate transition state theory, and pressure effects were estimated with the system-specific quantum Rice-Ramsperger-Kassel theory; this allowed us to investigate the role of the complex by using the canonical unified statistical model. The formation and equilibration of the pre-reactive complex, which is also important at low pressures, enhances the reactivity by inducing a large tunneling effect that leads to a significant increase of the rate constants at cold and ultracold temperatures. These findings may help to understand and model the fate of complex organic molecules in the interstellar medium, and suggest an alternative route for the high energy barrier keto−enol tautomerism which otherwise is not kinetically favored at low temperatures.

1. INTRODUCTION

Biofuels like ethanol, and other alcohols like 2-butanol are an interesting alternative to gasoline and diesel, representing a renewable, clean, and efficient source of energy. This is the case of higher alcohols (e. g., butanols, pentanols), for which many theoretical and experimental studies have been conducted on their pyrolysis and oxidation characteristics as reviewed by Sarathy *et al*.[1]

In order to optimize the combustion and pyrolysis processes of fuels and reduce their polluting emissions, a detailed understanding of the chemical reactions that rule their reactivity as well as the intermediates formed during those processes becomes critical. Kinetic models are useful tools to achieve these goals, but their performance strongly depends on how well the kinetics of those reactions is described. The tautomerism keto–enol, in which the keto form is usually favoured due to its larger stability, is an important process in the pyrolysis and combustion of alcohols and in hydrocarbon oxidation,[2] and thereby these reactions are of especial interest in the development of kinetic models for those species.[1,3]

We recently updated[4] Sarathy's model[1] by calculating the rate constants for the forward and reverse reaction of the unimolecular keto–enol tautomerism that converts propen-2-ol (i-C_3H_5OH) into acetone (CH_3COCH_3),

$$\text{i-}C_3H_5OH \Leftrightarrow CH_3COCH_3 \qquad \text{(R1)}$$

and obtained what we call hereafter *former model*. In the original model, Sarathy *et al*. used for reaction R1 the rate constants for the conversion of vinyl alcohol into acetaldehyde[5] as an analogy, $k(1300\ K) = 3.36 \cdot 10^3$ s^{-1}; our calculated values in the high-pressure limit, using high level *ab initio* and multi-structural torsional transition state theory calculations with tunneling corrections, are larger, $k(1300\ K) = 3.21 \cdot 10^4$ s^{-1},[4] indicating that this analogy is not very appropriate. As a result, closed batch reactor simulations for the pyrolysis of tert- (t-C_4H_9OH) and 2-butanol (s-C_4H_9OH) using our calculated rate constants predicted a larger yield of acetone and a quicker consumption of propen-2-ol than those using the analogy. The unimolecular tautomerism R1 turned out to be a prominent pathway for the production of acetone, in line with the findings by Yasunaga *et al*.[6]

Given the important role of the abovementioned keto–enol tautomerism in the combustion and pyrolysis of alcohols, the present work is aimed to further update kinetic models for butanol isomers in order to avoid the use of analogue reactions for those processes. Specifically, we investigated the HO_2-catalyzed keto–enol tautomerism that converts propen-2-ol into acetone,

$$\text{i-}C_3H_5OH + HO_2 \Leftrightarrow CH_3COCH_3 + HO_2 \qquad \text{(R2)}$$

This reaction is included in current kinetic models by means of an analogy, adopting the rate constants calculated by da Silva and Bozzelli[7] for the HO_2-catalyzed tautomerism that involves vinyl alcohol (CH_2=CHOH) and acetaldehyde (CH_3CHO),

$$CH_2{=}CHOH + HO_2 \Leftrightarrow CH_3CHO + HO_2 \quad (R3)$$

who found that the reaction R3 can be rapid at combustion temperatures as long as the levels of the HO_2 radical are suitably high. Because the unsaturated alcohol i-C_3H_5OH is present in the combustion of butanol isomers, an investigation similar to that of da Silva and Bozzelli is warranted for the reaction R2.

The HO_2 radical is an important species not only in combustion, but also in the atmosphere and interstellar medium. In addition, different alcohols have been detected in interstellar clouds, some of them in large amounts. Tuner and Apponi detected vinyl alcohol in the molecular cloud Sagittarius B2,[8] and large amounts of methanol have been reported by Harvey-Smith and Cohen in the W3(OH) region of our galaxy.[9] Measurements of C_3H_6O isomers have reported the presence of acetone[10,11] and propionaldehyde;[12,13] given the role of isomerism at interstellar conditions, propen-2-ol may be present as well.[14] Thus, a detailed kinetic study of the reaction R2 at low temperatures and pressures is also important to understand in what extent these keto–enol tautomerisms take place in the atmosphere and contribute to the consumption and formation of complex organic molecules in interstellar clouds.

In this work, we have characterized the potential energy surface (PES) of the reaction i-$C_3H_5OH + HO_2 \Leftrightarrow CH_3COCH_3 + HO_2$ by means of electronic structure calculations at the CCSD(T)/aug-cc-pVTZ //M06-2X/cc-pVTZ level. Rate constants have been calculated within the multi-structural torsional variational transition state theory framework, including tunneling corrections. The calculated rate constants for the tautomerism R2 were implemented in the former model recently developed by us,[4] which describes that tautomerism using the analogue reaction R3, resulting in a new version referred to as *updated model*. Both, former and updated models, were used to simulate the combustion of s-C_4H_9OH, allowing us to analyse the role of the studied reaction in the combustion of that butanol isomer as well as in the overall keto–enol tautomerism converting propen-2-ol into acetone.

We draw some conclusions about the atmospheric implications of the catalyzer HO_2 by comparing its catalytic performance to that of other species like formic acid, HCOOH, which has been also proven to catalyse the studied tautomerism,[15] and also by considering the levels of HO_2 in the atmosphere.

Finally, we shed light into the role of the intermediate complex found on the entry channel of the PES of the reaction R2, hereafter called Complex-1, at very low temperatures when tunnelling effect becomes very important; to do so, we calculated the association rate constants for the formation of Complex-1 by using the variable reaction coordinate transition state theory and the canonical unified statistical model (CUS),[16] considering the following step-wise mechanism

$$\text{i-}C_3H_5OH + HO_2 \Leftrightarrow \text{Complex-1} \rightarrow CH_3COCH_3 + HO_2 \quad (R4)$$

To investigate the role of Complex-1, which depends on the extent of its stabilization by collisions with other bodies, pressure effects were also considered with the system-specific quantum Rice-Ramsperger-Kassel theory (SS-QRRK).

2. COMPUTATIONAL DETAILS

2.1. *Ab initio* calculations. We performed electronic structure calculations at the CCSD(T)/aug-cc-pVTZ//M06-2X/cc-pVTZ level of theory using the Gaussian09 package[17] to explore the potential energy surface (PES) of the reaction i-C_3H_5OH + HO_2 ⇔ CH_3COCH_3 + HO_2. For the geometry optimizations and frequencies calculations we used the M06-2X method[18] and the cc-pVTZ basis set;[19] the energy was refined using the CCSD(T) method[20] with the aug-cc-pVTZ basis set.[19]

The minimum energy path (MEP) was calculated with the Gaussrate-2016 code[21] over the reaction coordinate range -2.4 bohr to +2.4 bohr, with a stepsize of 0.1 bohr in mass-scaled coordinates and a scaling mass equal to 1 amu; the Page and McIver's algorithm[22] was used. A stepsize of $4.72 \cdot 10^{-2}$ bohr was used between -0.52 bohr and 0.52 bohr for a better description of the area near the saddle point, which is critical in determining the variational transition state and the tunneling contribution; hessian was evaluated every third step, and the normal modes along the MEP were defined by using interanl coordinates. This allowed us to calculate the vibrationally adiabatic potential energy curve, $V_a^G(s)$, which was also used for the tunneling transmission coefficient calculations

$$V_a^G(s) = V_{MEP}(s) + ZPE(s) \quad (1)$$

where $V_{MEP}(s)$ and $ZPE(s)$ are the classical potential energy and zero point energy, respectively, as function of the reaction coordinate s.

2.2. High-pressure limit rate constants calculations. The calculations of the forward, $k_{MS-T(C),f}^{CVT/SCT}$, and reverse, $k_{MS-T(C),r}^{CVT/SCT}$, rate constants (in units of cm^3 $molecule^{-1}$ s^{-1}) for the concerted mechanism of the reaction i-C_3H_5OH + HO_2 ⇔ CH_3COCH_3 + HO_2 were carried out with the multi-structural variational transition state theory with torsional anharmonicity and a coupled torsional potential, MS-T(C).[23,24] The kinetic calculations were performed with the Polyrate-2016 code.[25] To account for the effect of the multiple conformers of the reactants and saddle point on the rate constants, also known as multi-structural anharmonicity, we used MSTor.[26] The term "conformers" refers to distinguishable structures that can be converted into each other by internal rotations.

Under the MS-T(C) scheme, the conformational rovibrational partition function is defined as

$$Q_{con-rovib}^{MS-T(C)} = \sum_{j=1}^{J} Q_{rot,j} exp(-\beta U_j) Q_j^{HO} \prod_{\eta=1}^{t} \bar{f}_{j,\eta} \quad (2)$$

The set of conformers of each species (reactant or saddle point) is labeled as *J*, being *j=1* the conformer with the lowest potential energy or global minimum; the potential energy of each conformer, U_j, is defined with respect to that of the global minimum, thus $U_{j=1}= 0$. $Q_{rot,j}$ is the classical rotational partition function, and the factor β is $1/k_bT$; k_b is the Boltzmann's constant. The normal-mode harmonic oscillator partition function, Q_j^{HO}, is adjusted to introduce the torsional anharmonicity associated to the coupled torsion η by the term $\bar{f}_{j,\eta}$, and it is given by

$$Q_j^{HO} = \exp(-h\omega/2k_bT)[1 - \exp(-h\omega/k_bT)]^{-1} \quad (3)$$

In Eq. (3), h, ω, and T are the Planck's constant, frequency and temperature, respectively.

The product term of Eq. (2) is defined as

$$\prod_{\eta=1}^{t} \bar{f}_{j,\eta} = (2\pi\hbar\beta)^{t/2} \frac{\prod_{m=1}^{F} \omega_{j,m}}{\prod_{\bar{m}=1}^{F-t} \bar{\bar{\omega}}_{j,\bar{\bar{m}}}} \frac{\sqrt{det\boldsymbol{D}_j}}{\prod_{\tau=1}^{t} M_{j,\tau}} \prod_{\eta=1}^{t} \exp\left(-\frac{\beta W_{j,\eta}^{(C)}}{2}\right) I_0\left(\frac{\beta W_{j,\eta}^{(C)}}{2}\right) \quad (4)$$

where $\bar{\bar{\omega}}_{j,\bar{\bar{m}}}$ and $\boldsymbol{D}_j$ are the torsion-projected normal mode frequencies and the Kilpatrick and Pitzer torsional moment of inertia matrices, respectively. $M_{j,\tau}$ are the local periodicity parameters for uncoupled torsions τ, and I_0 is a modified Bessel function.

The effect of the multiple conformers is introduced by defining the multi-structural torsional anharmonicity factor $F_X^{MS-T(C)}$, where *X* stands for the species involved in the reaction, that is, reactants, $F_R^{MS-T(C)}$, or saddle point, $F_{SP}^{MS-T(C)}$

$$F_X^{MS-T(C)} = Q_{con-rovib,X}^{MS-T(C)} / Q_{con-rovib,X,j=1}^{SS-T(C)} \quad (5)$$

The term $Q_{con-rovib,X,j=1}^{SS-T(C)}$ is the single-structural rovibrational partition function for the global minimum conformer of the species *X*, including torsional anharmonicity and coupled torsion, and is given by

$$Q_{con-rovib,j}^{SS-T(C)} = Q_{rot,j} exp(-\beta U_j) Q_j^{HO} \prod_{\eta=1}^{t} \bar{f}_{j,\eta} \quad (6)$$

The multi-structural torsional anharmonicity factors for the reactant and saddle point, $F_R^{MS-T(C)}$ and $F_{SP}^{MS-T(C)}$, allow us to compute that factor for the reaction,

$$F^{MS-T(C)} = F_{SP}^{MS-T(C)} / F_R^{MS-T(C)} \quad (7)$$

In the calculation of the partition functions we used scaled vibrational frequencies by a factor of 0.955[27] in order to improve the description of the torsional anharmonicity as well as to obtain a more accurate adiabatic potential energy curve ($V_a^G(s)$). Quantum effects on the reaction coordinate were included with the small-curvature tunneling approach (SCT),[25] obtaining the transmission coefficients κ^{SCT}. The final rate constant has been calculated as

$$k_{MS-T(C)}^{CVT/SCT} = \kappa^{SCT}\Gamma\frac{k_b T}{h}\frac{Q_{elec}^{\neq}Q_{con-rovib}^{MS-T(C),\neq}}{\Phi_t Q_{elec}^{R}Q_{con-rovib}^{MS-T(C),R}}\exp(-\beta V^{\neq}) \quad (8)$$

where the superscripts ≠ and *R* stand for conventional transition state and reactants, respectively, and $V^{\neq}$ is the classical barrier height defined with the global minimum conformers. The factor Γ is the recrossing transmission coefficient, given by the ratio of the CVT rate constant to the TST one; CVT and TST stand for canonical variational and transition state theories, respectively. The relative translational and electronic partition functions are denoted as Φ_t and $Q_{elec}^{R}/Q_{elec}^{\neq}$, respectively. The terms κ^{SCT} and Γ are calculated using the global minimum structures and the harmonic oscillator approach.

For the calculation of the periodicity parameters $M_{j,\tau}$, which are necessary to evaluate the multi-structural rovibrational partition functions (Eq. (2)) and thus the multi-structural anharmonicity factors (Eq. (5)), we used the schemes NS:SC = 3:0, 1:0, and 0:2 for the species i-C_3H_5OH, saddle point, and CH_3COCH_3, respectively, where NS and SC respectively mean nearly separable and strongly coupled. The two torsions of the methyl groups of the species CH_3COCH_3 are strongly coupled, and thus the Voronoi tessellation method implemented in MSTor was used. For the i-C_3H_5OH and saddle point species, without coupled torsions, the parameters $M_{j,\tau}$ could be determined manually.

As for the step-wise mechanism R4, i-C_3H_5OH + HO_2 ⇔ Complex-1 → CH_3COCH_3 + HO_2, the high-pressure limit rate constants for the barrier-less association of the reactants to form Complex-1 were calculated by using the variable reaction coordinate transition state theory, VRC-VTST,[28,29] as implemented in Polyrate. This formulation of the transition state theory is appropriate for barrier-less association reactions in which the determination of the dividing surface is not straightforward. The rate constants were variationally determined by minimizing the number of transitional states *N(E,J,s)* as function of the total energy, *E*, angular momentum, *J*, and reaction coordinate, *s*, yielding an *E* and *J* resolved reactive flux, $N(E,J,s)^{E,J-\mu VT}$, within the variable reaction coordinate VRC-*E*,*J*-μVT.

Under the VRC-VTST formulation, the normal modes are sorted into two different kinds, conserved and transitional modes. The former are the internal vibrational modes of the reacting fragments, i-C_3H_5OH and HO_2, whose character barely changes during the course of the reaction. The latter corresponds to the rotations of both fragments and their relative motion, which become vibrations and overall rotations as the two fragments approach to each other inducing bond formation.

The variable reaction coordinate *s* was set by defining a single-faceted dividing surface determined by two pivot points, one for each of the reacting fragments (see Figure 1). Pivot point 1 is equidistantly located along the line connecting the hydrogen atoms of the moieties −OH and =CH_2 of the fragment i-C_3H_5OH; pivot point 2 is also equidistantly located along the line connecting the O and H terminal atoms of the fragment HO_2. Both pivot points are separated by a distance r_{12} during the course of the reaction, so that

$s = r_{12}$, and the reactive flux was variationally minimized within the interval 3.5 Å ≤ *s* ≤ 5.6 Å, also varying the location of the pivot points from its original location (Figure 1) up to a distance *d* of 0.1 Å along the perpendicular to the plane formed by the −OH and =CH_2 moieties (pivot point 1, i-C_3H_5OH fragment), and along the plane formed by the O, O, and H atoms perpendicularly to the O and H terminal ones (pivot point 2, HO_2 fragment). The distances *s* and *d* were scanned using intervals of 0.1 Å and 0.02 Å, respectively. For each combination of the parameters *s* and *d*, an ensemble of 1000 configurations were examined in order to determine an average flux $N(E,J,s)^{E,J-\mu VT}$ for each dividing surface. The high-pressure limit rate constant for the association reaction (in units of cm^3 $molecule^{-1}$ s^{-1}) is determined as

$$k_{ass}^{E,J-\mu VT}(T,s) = \frac{\hbar^2}{2\pi} g_e \frac{\sigma_1 \sigma_2}{\sigma^{\neq} Q_1 Q_2} \left(\frac{2\pi}{\mu k_B T}\right)^{3/2} \int e^{-E/k_B T} N(E,J,s)^{E,J-\mu VT} dE dJ \quad (9)$$

where g_e is the ratio of the electronic partition function of the transition state to the product of the electronic partition functions of the reactants, Q_1 and Q_2 are the rotational partition functions of the reactants without symmetry numbers, which are included as $\sigma^{\neq}$, σ_1, and σ_2 for the transition state and reactants, respectively, and $\hbar$ is the reduced Planck's constant. Additional details on the calculations performed under the VRC-VTST theory can be found elsewhere.[25,28,29]

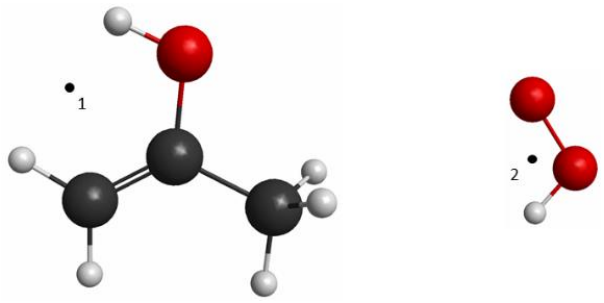

Figure 1. Location of the pivot points 1 and 2 in fragments i-C_3H_5OH and HO_2, respectively, for the definition of the single-faceted dividing surface for the VRC-*E,J*-μVT calculations.

As we will see in the next Section, Complex-1 is stabilized by conventional O···H and particularly strong OH···π type hydrogen bonds between the HO_2 radical and the −OH and =CH_2 moieties of i-C_3H_5OH. A more appropriate description of the dividing surface to the formation of the complex might be by defining a multi-faceted dividing surface with several pivot points for each fragment, that is, one for each binding site in order to describe the different intermolecular interactions that drive the double hydrogen atom transfer reaction. However, the presence of several heavy atoms and the large number of electronic structure calculations necessary to obtain the average flux make the calculations computationally expensive, and thus we opted for a single-faceted dividing surface. Given that the approach of the HO_2 radical can take place

along any of the faces of the double bond of i-C_3H_5OH, the final reactive flux, and thus the rate constants, were multiplied by two. In addition, in order to make the VRC-*E*,*J*-μVT calculations computationally feasible, we used the M06-2X/6-311++G(2df,2pd) level of theory for the study of the step-wise mechanism, which still implies a relatively large basis set (larger than cc-pVTZ). Both, the higher level CCSD(T)/aug-cc-pVTZ//M06-2X/cc-pVTZ and the lower level M06-2X/6-311++G(2df,2pd) predict very similar potential energy profiles, validating the use of the abovementioned computationally feasible level of theory for the VRC-*E*,*J*-μVT calculations.

Finally, the high-pressure limit rate constants for the conversion of Complex-1 into the products CH_3COCH_3 and HO_2, $k_{MS-T(C),2}^{CVT/SCT}$ (in units of s^{-1}), were calculated with the MS-T(C) theory. Both, $k_{ass}^{E,J-\mu VT}$ and $k_{MS-T(C),2}^{CVT/SCT}$, were based on M06-2X/6-311++G(2df,2pd) electronic structure calculations.

2.3. Pressure dependent rate constants calculations. Pressure effects were included in the high-pressure limit association rate constants $k_{ass}^{E,J-\mu VT}$ by using the chemical activation mechanism for a bimolecular association reaction; the calculations were carried out using SS-QRRK theory,[30] implemented as a utility code in Polyrate.[25] This method applies the steady-state approximation to the chemical activation mechanism, yielding the following pressure dependent association rate constant

$$k_{stab} = k_{ass}^{E,J-\mu VT} \sum_{E_o}^{+\infty} \frac{k_c[M] f(E)}{k_c[M] + k_{-1}^{QRRK}(E)} \tag{10}$$

where [M] is the concentration of the bath gas (calculated using the ideal gas law), E_o is the threshold energy of the dissociation of Complex-1 to form the reactants, k_c is the collisional deactivation rate constant for the activated complex Complex-1*, $f(E)$ is the fraction of energized species of Complex-1* at energy E, and $k_{-1}^{QRRK}(E)$ is a QRRK energy-resolved rate constant for the dissociation back to reactants of Complex-1. They are calculated as

$$k_c(T) = Z\beta_c \tag{11}$$

$$f(E) = \frac{k_{-1}^{QRRK}(E) K(E)}{\sum_{E_o}^{+\infty} k_{-1}^{QRRK}(E) K(E)} \tag{12}$$

$$k_{-1}^{QRRK}(E) = A^{QRRK} \frac{n!\,(n-m+s-1)!}{(n-m)!\,(n+s-1)!} \tag{13}$$

where

$$K(E) = exp\left(\frac{-nhv}{k_bT}\right)\left[1 - exp\left(\frac{-hv}{k_bT}\right)\right]^s \frac{(n+s-1)!}{n!\,(s-1)!} \tag{14}$$

$$A^{QRRK} = k_{diss}^{E,J-\mu VT}(T) exp\left(\frac{E_{diss}^{E,J-\mu VT}(T)}{RT}\right) \tag{15}$$

$$m = E_{diss}^{E,J-\mu VT}/hc\bar{v} \quad (16)$$

A^{QRRK} is the frequency factor, Z and β_c are the Lennard-Jones collision rate constant and the collision efficiency, respectively, n is the number of quanta excited at energy E, m is the number of quanta excited at energy E_o, and s is the number of vibrational degrees of freedom of Complex-1. $k_{diss}^{E,J-\mu VT}$ and $E_{diss}^{E,J-\mu VT}$ are the thermal rate constant and activation energy for the dissociation of Complex-1 into the reactants, respectively.

First, we obtained $k_{diss}^{E,J-\mu VT}$ from the calculated $k_{ass}^{E,J-\mu VT}$ and the concentration equilibrium constant, defined as

$$K_{C,diss} = \frac{k_{diss}^{E,J-\mu VT}}{k_{ass}^{E,J-\mu VT}} \quad (17)$$

and second, we fitted the high-pressure limit rate constants $k_{diss}^{E,J-\mu VT}$ to the following equation

$$k = A\left(\frac{T}{300}\right)^n exp\left[-\frac{E(T+T_o)}{R(T^2+T_o^2)}\right] \quad (18)$$

and determined the fitting parameters A, n, E, and T_o. These fitting parameters were then used to determine the threshold energy E_o, which is set equal to the high-pressure limit Arrhenius activation energy for the dissociation reaction, $E_{diss}^{E,J-\mu VT}$

$$E_{diss}^{E,J-\mu VT} = \frac{E(T^4 + 2T_oT^3 - T_o^2T^2)}{(T^2+T_o^2)^2} + nRT \quad (19)$$

Using the values yielded by Eq. (19), A^{QRRK} can be calculated by using Eq. (15), so that k_{stab} can be also estimated. We obtained negative values for $E_{diss}^{E,J-\mu VT}$, which would result in $k_{-1}^{QRRK}(E)$ values larger than the frequency factor A^{QRRK}; this nonphysical behaviour was fixed by assuming that $E_{diss}^{E,J-\mu VT} = 0.0$ kcal mol^{-1}, and therefore $k_{-1}^{QRRK}(E)$ would adopt the maximum possible value which is that of the frecuency factor A^{QRRK}, that is, $A_{uni}^{\infty}(T)$.

To compute the Lennard-Jones collision rate constant we used the Lennard-Jones parameters for n-propanol σ = 4.549 Å and ε/k_b = 576.7 K, which have been used in other works for propen-2-ol systems.[4] Those for the bath gas Ar are σ = 3.542 Å and ε/k_b = 93.3 K. The collision efficiency was calculated with a de-activation averaged energy transferred value of $< \Delta E >_{down}$= 400 cm^{-1}, which is a common value for the gas Ar;[31,32] nevertheless, a sensitivity analysis on this parameter was performed to check its effect on the calculated rate constants.

2.4. Numerical simulations of the combustion of s-C_4H_9OH. We implemented the rate constants for the reaction i-C_3H_5OH + HO_2 ⇔ CH_3COCH_3 + HO_2 in the kinetic model for butanol isomers recently updated by us (former model)[4] to assess the impact of the studied HO_2-catalyzed tautomerism not only in the

combustion of 2-butanol (s-C_4H_9OH), but also in the overall keto–enol tautomerism that converts propen-2-ol into acetone. Simulations were performed in a closed batch reactor and a perfectly stirred reactor (JSR) with the ANSYS CHEMKIN-PRO 18.1 software[33] and the performance of the former and updated kinetic models was compared.

For the closed batch reactor simulations, the initial conditions were 1.9 atm and temperatures of 700, 800, and 1300 K (similar to those used in the shock tube pyrolysis experiments by Yasunaga *et al*.[6] but extended to lower temperatures) for stoichiometric mixtures of fuel:air. As for the JSR simulations, s-C_4H_9OH was diluted in O_2 and N_2 with molar fractions 0.01:0.1:0.89 at 1 atm and temperatures in the 800–1200 K range, with a residence time of 2 seconds.

3. RESULTS AND DISCUSSION

3.1 Stationary points and topology of the PES. The adiabatic potential energy profile, which includes ZPE corrections, of the reaction i-C_3H_5OH + HO_2 ⇔ CH_3COCH_3 + HO_2 at the CCSD(T)/aug-cc-pVTZ//M06-2X/cc-pVTZ level is shown in Figure 2. Two conformers, separated by 1.45 kcal mol^{-1}, were found for the i-C_3H_5OH reactant when the H–O–C–C dihedral angle was rotated. The saddle point and Complex-1 have a non-superimposable mirror image (enantiomer), equivalent in energy (not shown in Figure 2), as the result of the attack of the HO_2 radical along the other side of the double bond. No conformers were found for the CH_3COCH_3 product. All the conformers were included in the calculation of the rate constants, as was explained in Section 2.2.

The multi-reference character of the stationary points was addressed by means of the T1 diagnostic.[34] All the stationary points but the HO_2 radical show T1 values lower than 0.02, indicating that the static correlation is not a problem. For the HO_2 radical, this magnitude shows a value of 0.028, which is also much lower than the value of 0.04 considered as acceptable for open-shell systems. We therefore concluded that a single-reference treatment is appropriate.

The radical HO_2 promotes a concerted double hydrogen atom transfer reaction which induces a low barrier height to the tautomerism; this barrier height is 46.71 kcal mol^{-1} lower than that to the unimolecular tautomerism i-C_3H_5OH ⇔ CH_3COCH_3 we calculated in our previous work.[4] The standard free energy barriers of the HO_2-catalyzed and non-catalyzed tautomerisms are 17.9 and 53.64 kcal mol^{-1}, respectively. The potential energy profile plotted in Figure 2 also shows two intermediate complexes, Complex-1 and Complex-2, located in wells of -7.18 and -22.09 kcal mol^{-1}, respectively. Both complexes are stabilized by hydrogen bonds between the HO_2 radical and the molecules i-C_3H_5OH or CH_3COCH_3, but the electronic structure of Complex-1 shows some special features that deserve special attention.

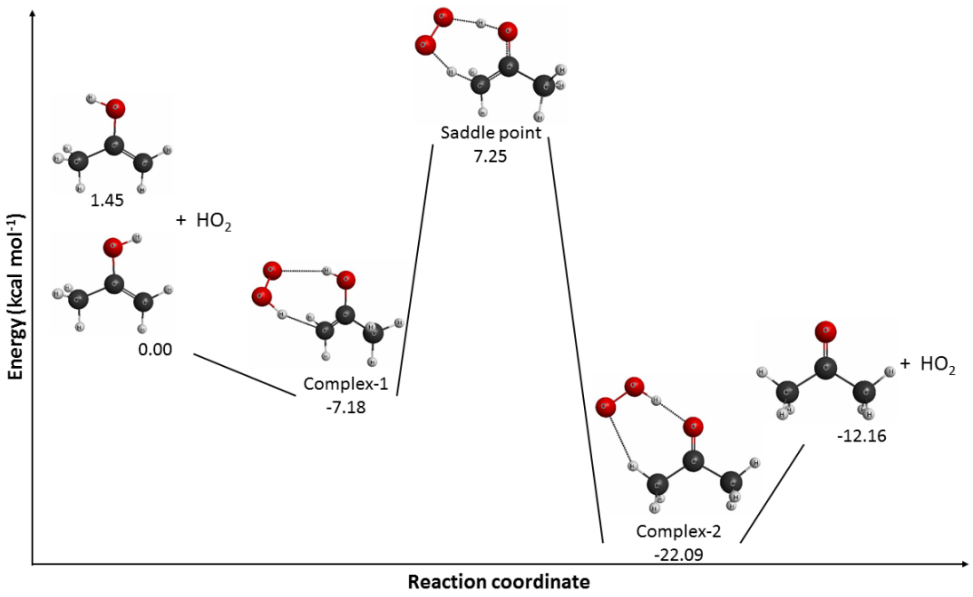

Figure 2. CCSD(T)/aug-cc-pVTZ//M06-2X/cc-pVTZ adiabatic potential energy profile (kcal mol^{-1}) of the reaction i-C_3H_5OH + HO_2 ⟺ CH_3COCH_3 + HO_2. The energy is defined with respect to the energy of the global minimum structures of the reactants. Carbon, oxygen and hydrogen atoms are shown in black, red and white, respectively.

We performed a natural bond orbital (NBO) analysis on the optimized geometry of Complex-1, shown in Figure 3, with the Gaussian09 package[17] in order to determine the nature of the intermolecular interactions between the fragments HO_2 and i-C_3H_5OH. NBOs can be sorted into one center localized (lone pairs) and two center localized (bonds) orbitals as in a Lewis structure, and they are obtained by the transformation of the canonical orbitals of the basis set using atomic natural and natural hybrid orbitals (ANO and NHO). We analyzed the interactions between the antibonding, bonding, and lone pair orbitals of both fragments, and identified two kinds of hydrogen bonds. The first one is a conventional hydrogen bond HO−O(13)···H(10)−OC which results from the interaction between the lone pair orbitals of the atom O(13) and the antibonding orbital associated with the H(10)–O(9) bond, $n_{O(13)} \rightarrow \sigma^*_{H(10)-O(9)}$, with stabilization energies as high as 1.78 kcal mol^{-1}. The second one is an OO−H(12)···π hydrogen bond resulting from the interaction of the π electron density of the C(1)=C(6) double bond and the antibonding orbital associated with the H(12)–O(11) bond, $\pi_{C(1)=C(6)} \rightarrow \sigma^*_{H(12)-O(11)}$. This π electron density is perpendicular to the double bond, and thus is located along the approaching axis of the HO_2 radical, favouring an even stronger interaction with stabilization energies as high as 3.96 kcal mol^{-1}. The net result of the described intermolecular interactions is a large stabilization of the intermediate Complex-1.

The O−H···π hydrogen bond, and its analogues N−H···π and C−H···π, have been reported as weak interactions that induce to some stabilization[35-37] and have implications in the folding of biomolecules.[36] However, they are not usually as strong as conventional hydrogen bonds, which is in stark contrast to our findings on Complex-1, wherein the O−H···π hydrogen bond stabilizes the complex to a larger extent. The strong interaction between the fragments HO_2 and i-C_3H_5OH in Complex-1 can be also exemplified by the large vibrational frequency of the intermolecular stretching mode, with a value of 232 cm^{-1}; this value is larger than, for example, that reported by Mukhopadhyay *et al*. for the C−H···π bonded complex formed by p-fluorophenol and 2,5-dihydrofuran,[37] with a value of 213 cm^{-1}. The eigenvector of this normal mode is also represented in Figure 3; it can be seen that it is exclusively localized along the intermolecular stretching coordinate. The reason why the O−H···π hydrogen bond is remarkably strong might be the more pronounced acidity of the O(11)–H(12) group due to the larger polarization of the O–H bond compared to its C–H and N–H counterparts.

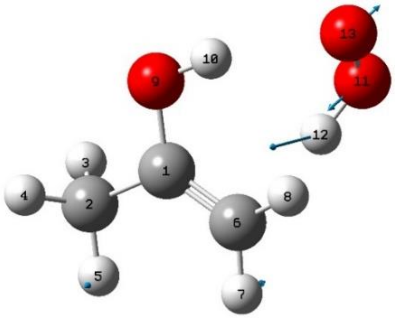

Figure 3. CCSD(T)/aug-cc-pVTZ//M06-2X/cc-pVTZ optimized geometry of Complex-1. The eigenvector of the intermolecular stretching mode (232 cm^{-1}) is also shown.

3.2. Rate constants calculations. We first calculated the multi-structural torsional anharmonicity factors for the species i-C_3H_5OH, saddle point, and CH_3COCH_3. For the reactant i-C_3H_5OH, with two non-equivalent conformers, this factor is 1 at low temperatures (200 K) and becomes 2 as temperature increases and makes the higher energy conformer energetically accessible. The species saddle point and CH_3COCH_3, with two equivalent and zero conformers, respectively, show values for this factor of 2 and 1 across the entire temperature range, respectively. As a result, $F^{MS-T(C)}$ for the forward reaction varies from 2 at 200 K to 1 in the limit of high temperatures, while that for the reverse reaction shows a constant value of 2.

With the factors $F^{MS-T(C)}$, the rate constants for the forward and reverse reactions i-C_3H_5OH + HO_2 ⇔ CH_3COCH_3 + HO_2 were calculated. These rates, including tunneling and multi-structural torsional anharmonicity corrections, are plotted in Figure 4 and tabulated in Table 1; the rate constants calculated by da Silva and Bozzelli[7] for the analogue reaction CH_2=CHOH + HO_2 ⇔ CH_3CHO + HO_2 used in current

kinetic models are also represented in Figure 4 for comparison. Our calculated rate constants in the temperature range 200–3000 K were fitted to the following two-term Arrhenius equation (in $cm^3\ mol^{-1}\ s^{-1}$) in order to perform our simulations with CHEMKIN

$$k_{forward} = 1 \cdot 10^{-1} \cdot T^{3.1} \exp\left(-\frac{1600}{RT}\right) + 1.5 \cdot T^{3.0} \exp\left(-\frac{10000}{RT}\right) \quad (20)$$

$$k_{reverse} = 2 \cdot 10^{-6} \cdot T^{4.4} \exp\left(-\frac{11900}{RT}\right) + 3 \cdot 10^{2} \cdot T^{0.9} \exp\left(-\frac{11000}{RT}\right) \quad (21)$$

where R and T are the ideal gas constant and temperature with units of $cal\ mol^{-1}\ K^{-1}$ and K, respectively.

Tunneling in the reaction coordinate is relatively important in the studied reactions, especially in the reverse reaction due to its larger barrier height. At 200 K, the small curvature transmission coefficients κ^{SCT} of the forward and reverse reactions adopt values of $1.68 \cdot 10^3$ and $1.69 \cdot 10^5$, respectively. Tunneling effect rapidly vanishes as temperature increases.

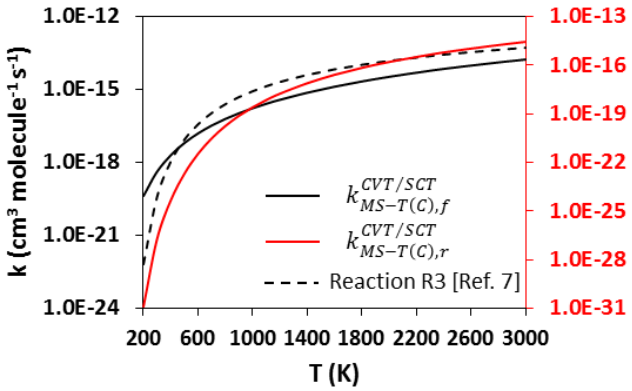

Figure 4. Plots of k (cm^3 $molecule^{-1}$ s^{-1}) *versus* T (K) of the calculated forward (black solid line, left y-axis) and reverse (red solid line, right y-axis) i-C_3H_5OH + HO_2 ⇔ CH_3COCH_3 + HO_2 reactions at the CCSD(T)/aug-cc-pVTZ//M06-2X/cc-pVTZ level. The forward rate constants of the analogue reaction CH_2=CHOH + HO_2 ⇔ CH_3CHO + HO_2 from Ref. (7) are also plotted (black dashed line, left y-axis).

The analogue reaction CH_2=CHOH + HO_2 ⇔ CH_3CHO + HO_2 (R3) used by Sarathy *et al.*[1] to describe the studied reaction in the original model is appropriate only at temperatures between 400 and 600 K. However, at lower and higher temperatures, which are respectively the regimes of interest in atmospheric and combustion chemistry, this analogy fails. For instance, at 200 and 1000 K the analogue forward rate constants are around 682 lower and 5 times higher, respectively, than the calculated forward rate constants for i-C_3H_5OH + HO_2 ⇔ CH_3COCH_3 + HO_2. We infer that the larger discrepancies observed at low temperatures are due to the larger sensitivity of the rate constants to the barrier height, which is not so important at high temperatures. Tunneling may be also responsible for those differences at low

temperatures. The observed discrepancies proves the usefulness of our calculated rate constants for the modelling of atmospheric and combustion processes. The analogue reaction used in current kinetic models may underestimate the role of the studied reaction in atmospheric modelling.

In Table 1 we also tabulate the high-pressure limit rate constants of the non-catalyzed tautomerism R1 previously calculated by us,[4] $k_{MS-T(C),Uni}^{CVT/SCT}$, for comparisson porposes. In order to compare $k_{MS-T(C),Uni}^{CVT/SCT}$ to the rate constants calculated in this work for the HO_2-catalyzed tautomerism, the latter should be converted into pseudo-first order rate constants by multiplying them by the concentration of the HO_2 radical, obtaining $k_{MS-T(C),Uni^*}^{CVT/SCT}$. To do so, we have assumed a concentration for the HO_2 radical in the atmosphere equal to $8 \cdot 10^8$ molecule cm^{-3}.[38] Under these conditions, the pseudo-first order HO_2-catalyzed reaction is more efficient in converting propen-2-ol into acetone than the unimolecular reaction at temperatures below 600 K; at higher temperatures, of interest in combustion, the opposite is true. Different concentrations of the HO_2 radical, which is assumed to be in general larger than the concentration of propen-2-ol, would change this picture.

Table 1. Thermal rate constants (cm^3 $molecule^{-1}$ s^{-1}) for the forward, $k_{MS-T(C),f}^{CVT/SCT}$, and reverse, $k_{MS-T(C),r}^{CVT/SCT}$, i-C_3H_5OH + HO_2 ⇔ CH_3COCH_3 + HO_2 reactions calculated at the CCSD(T)/aug-cc-pVTZ//M06-2X/cc-pVTZ level. The high-pressure limit rate constants for the non-catalyzed tautomerism calculated in our previous work,[4] $k_{MS-T(C),Uni}^{CVT/SCT}$ (s^{-1}), as well as the pseudo-first order rate constants for the HO_2-catalyzed tautomerism, $k_{MS-T(C),Uni^*}^{CVT/SCT}$ (s^{-1}), are also shown for comparisson purposes.

T (K)	$k_{MS-T(C),f}^{CVT/SCT}$	$k_{MS-T(C),r}^{CVT/SCT}$	$k_{MS-T(C),Uni}^{CVT/SCT}$	$k_{MS-T(C),Uni^*}^{CVT/SCT}$
200	$4.20 \cdot 10^{-20}$	$6.09 \cdot 10^{-32}$	$1.10 \cdot 10^{-21}$	$3.36 \cdot 10^{-11}$
298	$4.10 \cdot 10^{-19}$	$8.18 \cdot 10^{-28}$	$8.45 \cdot 10^{-18}$	$3.28 \cdot 10^{-10}$
400	$2.02 \cdot 10^{-18}$	$2.28 \cdot 10^{-25}$	$2.27 \cdot 10^{-13}$	$1.61 \cdot 10^{-09}$
500	$6.43 \cdot 10^{-18}$	$1.02 \cdot 10^{-23}$	$2.07 \cdot 10^{-09}$	$5.14 \cdot 10^{-09}$
600	$1.60 \cdot 10^{-17}$	$1.73 \cdot 10^{-22}$	$3.75 \cdot 10^{-06}$	$1.28 \cdot 10^{-08}$
700	$3.36 \cdot 10^{-17}$	$1.56 \cdot 10^{-21}$	$1.23 \cdot 10^{-03}$	$2.69 \cdot 10^{-08}$
800	$6.28 \cdot 10^{-17}$	$9.08 \cdot 10^{-21}$	$1.11 \cdot 10^{-01}$	$5.02 \cdot 10^{-08}$
900	$1.08 \cdot 10^{-16}$	$3.86 \cdot 10^{-20}$	$3.93 \cdot 10^{00}$	$8.62 \cdot 10^{-08}$
1000	$1.73 \cdot 10^{-16}$	$1.30 \cdot 10^{-19}$	$7.13 \cdot 10^{01}$	$1.39 \cdot 10^{-07}$
1100	$2.65 \cdot 10^{-16}$	$3.66 \cdot 10^{-19}$	$7.85 \cdot 10^{02}$	$2.12 \cdot 10^{-07}$
1200	$3.87 \cdot 10^{-16}$	$9.00 \cdot 10^{-19}$	$5.90 \cdot 10^{03}$	$3.10 \cdot 10^{-07}$
1400	$7.54 \cdot 10^{-16}$	$4.01 \cdot 10^{-18}$	$1.46 \cdot 10^{05}$	$6.03 \cdot 10^{-07}$

1600	$1.34\cdot10^{-15}$	$1.33\cdot10^{-17}$	$1.67\cdot10^{06}$	$1.07\cdot10^{-06}$
1800	$2.20\cdot10^{-15}$	$3.57\cdot10^{-17}$	$1.14\cdot10^{07}$	$1.76\cdot10^{-06}$
2000	$3.41\cdot10^{-15}$	$8.26\cdot10^{-17}$	$5.34\cdot10^{07}$	$2.73\cdot10^{-06}$
2300	$6.06\cdot10^{-15}$	$2.35\cdot10^{-16}$	$3.34\cdot10^{08}$	$4.85\cdot10^{-06}$
2500	$8.51\cdot10^{-15}$	$4.26\cdot10^{-16}$	$8.98\cdot10^{08}$	$6.81\cdot10^{-06}$
2800	$1.34\cdot10^{-14}$	$9.21\cdot10^{-16}$	$3.06\cdot10^{09}$	$1.07\cdot10^{-05}$
3000	$1.76\cdot10^{-14}$	$1.45\cdot10^{-15}$	$6.06\cdot10^{09}$	$1.41\cdot10^{-05}$

To cast light into the role of the intermediate complex in the forward reaction of the studied keto−enol tautomerism, and thus in the value of the previously calculated rate constant $k_{MS-T(C),f}^{CVT/SCT}$, we calculated the rate constants of the barrier-less association reaction to the formation of Complex-1, $k_{ass}^{E,J-\mu VT}$, by running VRC-*E,J*-μVT calculations, and applied the CUS model which includes both free energy bottlenecks, that is, the outer bottleneck to the formation of Complex-1, and the inner bottleneck to the formation of the final products (used in the calculation of $k_{MS-T(C),f}^{CVT/SCT}$ and $k_{MS-T(C),r}^{CVT/SCT}$); the association rate constants $k_{ass}^{E,J-\mu VT}$ are tabulated in Table 2. The reverse reaction CH_3COCH_3 + HO_2 → Complex-1 is not a favored process compared to the forward one due to its much larger energy barrier. The rate constants $k_{ass}^{E,J-\mu VT}$ show very large values which monotonically decrease, within a small interval, as temperature increases.

Because VRC-*E,J*-μVT calculations are computationally demanding, specially if several heavy atoms are present as in the studied system, we used the lower level of theory M06-2X/6-311++G(2df,2pd). This level of theory was validated by comparisson to the higher level CCSD(T)/aug-cc-pVTZ//M06-2X/cc-pVTZ used for our previous calculations. The ZPE-corrected barrier height predicted by the higher level is 7.2 kcal mol^{-1}, while that of the lower level is 5.7 kcal mol^{-1}, that is, 1.5 kcal mol^{-1} lower. These differences are even smaller for the case of Complex-1 (this portion of the PES is the critical one in the VRC-*E,J*-μVT calculations), with ZPE-corrected energies (with respect to the reactants i-C_3H_5OH + HO_2) of -7.2 and -8.0 kcal mol^{-1} with the higher and lower level, respectively. However, these differences may pose a source of error in our calculations, as will be discussed later.

For the step-wise mechanism i-C_3H_5OH + HO_2 ⇔ Complex-1 → CH_3COCH_3 + HO_2, the CUS model defines the rate constant as

$$\frac{1}{k^{CUS}} = \frac{1}{k_{ass}^{E,J-\mu VT}} - \frac{1}{k_C} + \frac{1}{k_{MS-T(C),f}^{CVT/SCT}} \qquad (22)$$

where k_C is a rate constant calculated for a dividing surface that is located at the free energy minimum corresponding to Complex-1. In the studied reactive system, this complex is much lower in energy than the reactants and the saddle point that defines the inner bottleneck, and thus the term $1/k_C$ can be neglected.

The term $1/k_{ass}^{E,J-\mu VT}$ can be neglected as well given the very large values of $k_{ass}^{E,J-\mu VT}$; as a result, Eq. (22) leads to similar rate constant values to those calculated by considering only the inner free energy bottleneck, $k_{MS-T(C),f}^{CVT/SCT}$, which were also calculated at the M06-2X/6-311++G(2df,2pd) level to carry out this analysis. These results indicate that the studied reaction is controlled by the inner dividing surface over the temperature range 200–3000 K, and our approach to consider it as a direct mechanism is appropriate within that wide temperature range, validating our calculated rate constants (Table 1) for combustion and atmospheric modelling.

Table 2. Thermal rate constants $k_{ass}^{E,J-\mu VT}$ (cm^3 $molecule^{-1}$ s^{-1}) calculated at the M06-2X/6-311++G(2df,2pd) level.

T (K)	$k_{ass}^{E,J-\mu VT}$
200	$4.43 \cdot 10^{-09}$
298	$3.52 \cdot 10^{-09}$
400	$3.27 \cdot 10^{-09}$
500	$2.47 \cdot 10^{-09}$
600	$1.99 \cdot 10^{-09}$
700	$1.73 \cdot 10^{-09}$
800	$1.58 \cdot 10^{-09}$
900	$1.48 \cdot 10^{-09}$
1000	$1.42 \cdot 10^{-09}$
1100	$1.37 \cdot 10^{-09}$
1200	$1.33 \cdot 10^{-09}$
1400	$1.29 \cdot 10^{-09}$
1600	$1.26 \cdot 10^{-09}$
1800	$1.23 \cdot 10^{-09}$
2000	$1.21 \cdot 10^{-09}$
2300	$1.19 \cdot 10^{-09}$
2500	$1.17 \cdot 10^{-09}$
2800	$1.15 \cdot 10^{-09}$
3000	$1.14 \cdot 10^{-09}$

3.3. Role of the tautomerism i-C_3H_5OH + HO_2 ⇔ CH_3COCH_3 + HO_2 in the combustion of s-C_4H_9OH.

In order to assess the role of the calculated rate constants for the titled reaction at the CCSD(T)/aug-cc-

pVTZ//M06-2X/cc-pVTZ level, we compared the performance of the former and updated kinetic models in the combustion of s-C_4H_9OH by running closed batch reactor and JSR simulations with CHEMKIN.

The species concentration profiles of key species in the combustion of a stoichiometric mixture of s-C_4H_9OH:air at 1.9 atm and 1300 K in a closed batch reactor using the updated model are plotted in Figure 5. Despite the differences between our rate constants and those from the analogy at this temperature, the results predicted by the former model are similar and thus they are not shown. We observed that the reaction i-C_3H_5OH + HO_2 ⟺ CH_3COCH_3 + HO_2 does not play an important role, although it is responsible for a minor CH_3COCH_3 production. Instead, the unimolecular tautomerism i-C_3H_5OH ⟺ CH_3COCH_3 and the HCOOH-catalyzed tautomerism

i-C_3H_5OH + HCOOH ⟺ CH_3COCH_3 + HCOOH (R5)

play the major role in the consumption and production of i-C_3H_5OH and CH_3COCH_3, respectively. Although the unimolecular tautomerism has an adiabatic barrier that is 46.71 kcal mol^{-1} higher than that to the HO_2-catalyzed process, the former plays a role as long as temperature is high enough to promote reactivity by surmounting its barrier height. In addition, the catalyzed reactions require a large enough concentration of catalyzer, which might not be the case for the HO_2-catalyzed reaction (see Table 1). Despite the larger concentration of HO_2 compared to that of HCOOH (Figure 5), the reaction R5 plays a more important role because the catalytic effect of HCOOH is more pronounced and leads to a lower barrier height.

The reaction R5 is included in the model by analogy to the reaction of vinyl alcohol with HCOOH studied by da Silva,[15]

C_2H_3OH + HCOOH ⟺ CH_3CHO + HCOOH (R6)

who predicted a much lower activation energy and thus significantly larger rate constants. For instance, at temperatures of 298, 700, 1300 and 2000 K, the rate constants values reported by da Silva[15] for the reaction R6, and therefore adopted for the reaction R5 in the kinetic model, are, respectively, $1.28\cdot10^{-14}$, $2.67\cdot10^{-15}$, $4.57\cdot10^{-15}$ and $1.02\cdot10^{-14}$ cm^3 $molecule^{-1}$ s^{-1}, that is, $3.1\cdot10^4$, 79.5, 7.6 and 3.0 times higher than those calculated in this work for the studied reaction at the corresponding temperatures. This makes reaction R5 the second most prominent reaction in the consumption of i-C_3H_5OH and production of CH_3COCH_3 during the combustion of the fuel, contributing to make the HO_2-catalyzed reaction not competitive and unimportant. We have recently described a remarkable catalytic effect of carboxylic acids in other reactive systems of importance in atmospheric chemistry, which also promotes a concerted double hydrogen atom transfer reaction.[39] Our findings show that these acids might be an efficient catalyzer even at relatively low concentration (as that in the atmosphere), and that the role of the studied HO_2-catalyzed tatutomerism might

be subjected to an accurate study of the analogy used to describe its main competitive reaction, that is, the reaction R5. Similar simulations were run at 700 and 800 K and the same conclusions were drawn.

JSR simulations were performed for a lean mixture s-C_4H_9OH:O_2:N_2 with mole fractions 0.01:0.1:0.89 at 1.0 atm and 800 K using both kinetic models. The species concentration profiles of the species involved in the studied tautomerism, as well as that of the fuel s-C_4H_9OH, are represented in Figure 6. The differences between the two models are subtle, both predicting exactly the same results. The most important reaction consuming i-C_3H_5OH during the combustion process is the unimolecular reaction i-C_3H_5OH ⇔ CH_3COCH_3. With the former model, when half of the initial amount of fuel has been consumed and beyond, the HCOOH-catalyzed tautomerism becomes important too; however, before this reaction starts playing a role, the HO_2-catalyzed tautomerism consumes some i-C_3H_5OH (not observed with the updated model), although to a lesser extent than the non-catalyzed tautomerism. This is probably due to the low concentration of HO_2 radicals (see Table 1). JSR simulations were conducted at higher temperatures and similar results were observed.

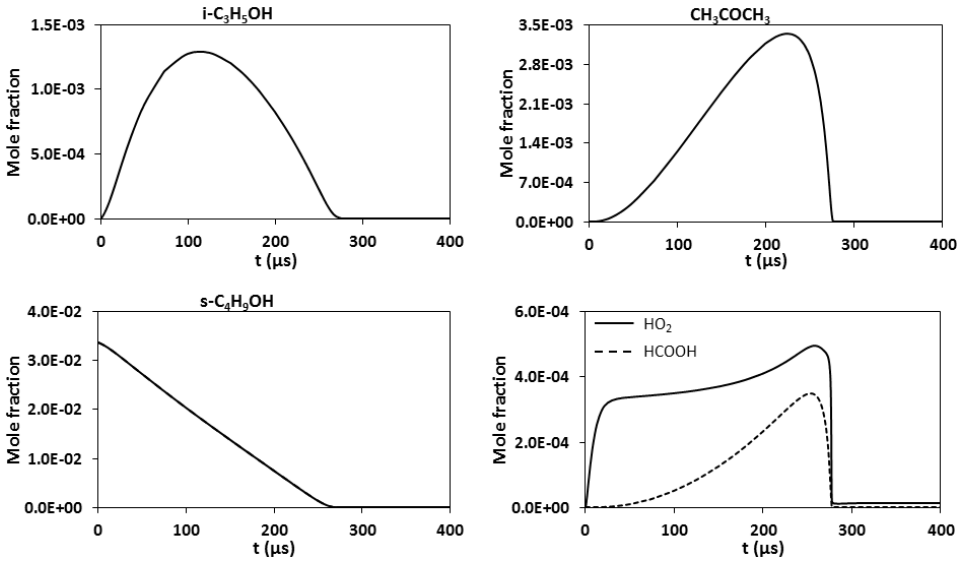

Figure 5. Species concentration profiles for key species in the combustion of a stoichiometric mixture s-C_4H_9OH:air at 1.9 atm and 1300 K using the updated model in a closed batch reactor.

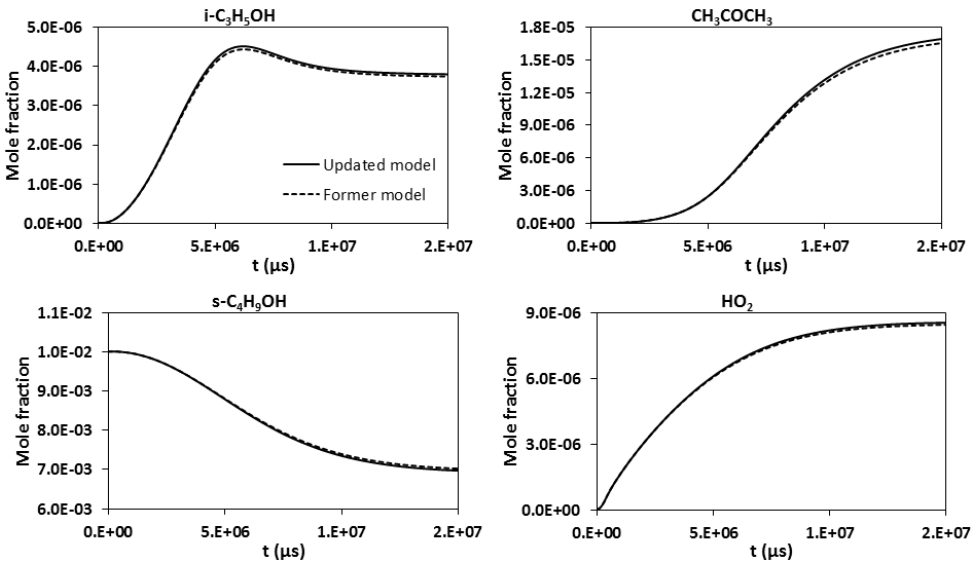

Figure 6. Species concentration profiles for key species in the combustion of a s-C_4H_9OH:O_2:N_2 mixture with mole fractions 0.01:0.1:0.89 at 1.0 atm and 800 K, using a JSR with the updated (solid line) and former (dashed line) models.

3.4. Rate constants calculations at ultracold temperatures. In Section 3.2 we demonstrated that considering the reaction i-C_3H_5OH + HO_2 ⟺ CH_3COCH_3 + HO_2 as a one-step mechanism with a single free energy bottleneck, and thus neglecting the effect of Complex-1 on the kinetics, is a good approach within the 200–3000 K temperature range. Nevertheless, under certain conditions of pressure and temperature, the role of this complex should be considered more carefully. If pressure is high enough, Complex-1 can be collisionally stabilized and equilibrated, and may become a long-lived intermediate complex. In addition, at very low temperatures quantum effects become important, and the double hydrogen atom transfer reaction studied in this work may be facilitated by tunneling through the barrier separating the equilibrated Complex-1 and the post-reactive Complex-2, which is significantly larger than that defined from the reactants i-C_3H_5OH + HO_2.

Assuming a collisionally and equilibrated pre-reactive intermediate complex, which is feasible in the high-pressure limit, the rate constant within the CUS model can be calculated by Eq. (22) but considering that tunneling can also take place at energies below and above those of the reactants i-C_3H_5OH + HO_2 and Complex-1, respectively. Therefore, the transmission coefficients κ^{SCT} were recalculated considering as the low energy limit the ground state energy of Complex-1, obtaining new values for $k_{MS-T(C),f}^{CVT/SCT}$, which are now labeled as $k_{MS-T(C),f}^{CVT/SCT^*}$. The rate constants $k_{MS-T(C),f}^{CVT/SCT^*}$ also include multi-structural torsional anharmonicity, and the only different between these rates and $k_{MS-T(C),f}^{CVT/SCT}$ is the way in which the

transmission coefficients were calculated, that is, κ^{SCT} or κ^{SCT^*}. The values of the magnitudes $k_{MS-T(C),f}^{CVT/SCT^*}$, κ^{SCT}, and κ^{SCT^*} are shown in Table 3, and the rate constants $k_{MS-T(C),f}^{CVT/SCT}$ and $k_{MS-T(C),f}^{CVT/SCT^*}$ are plotted for comparison in Figure 7 in the temperature range 100–3000 K. Additional details regarding the transmission coefficient calculations are provided in the supplementary information.

At temperatures above 500 K tunneling is essentially the same considering either the ground state of the reactants i-C_3H_5OH + HO_2 or that of Complex-1. However, as temperature decreases the differences become larger. For instance, at temperatures as low as 100 K, κ^{SCT^*} is $3.06 \cdot 10^{06}$ larger than κ^{SCT}. These differences are reflected in the rate constants plots of Figure 7, showing a non-Arrhenius behavior at temperatures below 250 K when Complex-1 is used as the lower energy limit to calculate the tunneling contribution. Non-Arrhenius temperature dependence is common in reactions with deep pre-reactive complexes and submerged barriers which make the activation energy becomes negative as temperature decreases.[40,41] In this case, the pre-reactive complex induces this non-Arrhenius behavior by facilitating the hydrogens transfer reaction by tunneling through the larger barrier that Complex-1 has to overcome after being stabilized and equilibrated in the high-pressure limit. At temperatures higher than 250 K, both models, that is, assuming that Complex-1 has or has not been stabilized, predict similar results; the differences arise at lower temperatures due to the prominence of the tunneling mediated mechanism.

Table 3. Transmission coefficients κ^{SCT} and κ^{SCT^*}, and thermal rate constants $k_{MS-T(C),f}^{CVT/SCT^*}$ (cm^3 $molecule^{-1}$ s^{-1}) at the M06-2X/6-311++G(2df,2pd) level.

T (K)	κ^{SCT}	κ^{SCT^*}	$k_{MS-T(C),f}^{CVT/SCT^*}$
100	$1.81 \cdot 10^{07}$	$5.54 \cdot 10^{13}$	$3.40 \cdot 10^{-14}$
150	$9.72 \cdot 10^{03}$	$1.43 \cdot 10^{06}$	$1.21 \cdot 10^{-17}$
200	$2.98 \cdot 10^{02}$	$1.86 \cdot 10^{3}$	$1.90 \cdot 10^{-18}$
250	$4.40 \cdot 10^{01}$	$8.88 \cdot 10^{01}$	$1.64 \cdot 10^{-18}$
298	$1.46 \cdot 10^{01}$	$1.96 \cdot 10^{01}$	$2.35 \cdot 10^{-18}$
400	$4.28 \cdot 10^{00}$	$4.51 \cdot 10^{00}$	$6.61 \cdot 10^{-18}$
500	$2.48 \cdot 10^{00}$	$2.50 \cdot 10^{00}$	$1.63 \cdot 10^{-17}$
600	$1.85 \cdot 10^{00}$	$1.85 \cdot 10^{00}$	$3.41 \cdot 10^{-17}$
700	$1.56 \cdot 10^{00}$	$1.56 \cdot 10^{00}$	$6.28 \cdot 10^{-17}$
800	$1.40 \cdot 10^{00}$	$1.40 \cdot 10^{00}$	$1.05 \cdot 10^{-16}$
900	$1.30 \cdot 10^{00}$	$1.30 \cdot 10^{00}$	$1.66 \cdot 10^{-16}$
1000	$1.24 \cdot 10^{00}$	$1.23 \cdot 10^{00}$	$2.48 \cdot 10^{-16}$

1100	$1.19 \cdot 10^{00}$	$1.19 \cdot 10^{00}$	$3.57 \cdot 10^{-16}$
1200	$1.16 \cdot 10^{00}$	$1.16 \cdot 10^{00}$	$4.97 \cdot 10^{-16}$
1400	$1.11 \cdot 10^{00}$	$1.11 \cdot 10^{00}$	$8.96 \cdot 10^{-16}$
1600	$1.09 \cdot 10^{00}$	$1.08 \cdot 10^{00}$	$1.49 \cdot 10^{-15}$
1800	$1.07 \cdot 10^{00}$	$1.07 \cdot 10^{00}$	$2.27 \cdot 10^{-15}$
2000	$1.05 \cdot 10^{00}$	$1.05 \cdot 10^{00}$	$3.22 \cdot 10^{-15}$
2300	$1.04 \cdot 10^{00}$	$1.04 \cdot 10^{00}$	$5.14 \cdot 10^{-15}$
2500	$1.03 \cdot 10^{00}$	$1.03 \cdot 10^{00}$	$6.78 \cdot 10^{-15}$
2800	$1.03 \cdot 10^{00}$	$1.03 \cdot 10^{00}$	$9.25 \cdot 10^{-15}$
3000	$1.02 \cdot 10^{00}$	$1.02 \cdot 10^{00}$	$1.12 \cdot 10^{-14}$

Variational effect, also known as recrossing Γ, was also evaluated within this wide temperature range as was explained in Section 2.2. This effect is not remarkable, specially at high temperatures, and varies from a factor of 1.68 at 100 K to a factor of 1.15 at 3000 K.

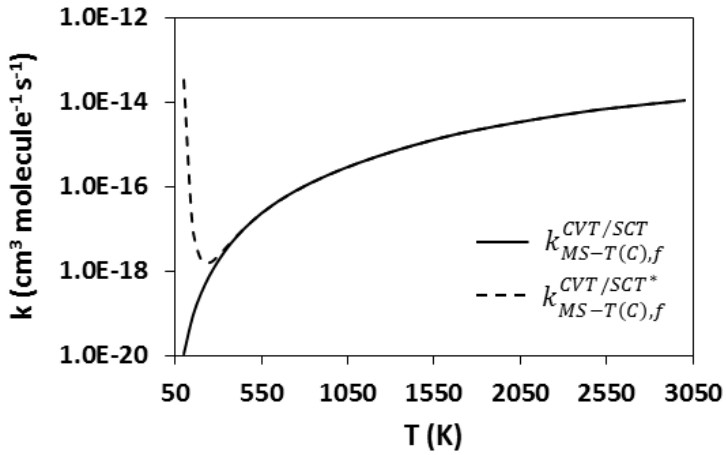

Figure 7. Plots of k (cm^3 $molecule^{-1}$ s^{-1}) *versus* T (K) of the M06-2X/6-311++G(2df,2pd) calculated forward rate constants of the reaction i-C_3H_5OH + HO_2 ⇔ CH_3COCH_3 + HO_2 considering the reactants i-C_3H_5OH + HO_2 ($k_{MS-T(C),f}^{CVT/SCT}$) and the intermediate Complex-1 ($k_{MS-T(C),f}^{CVT/SCT^*}$) as the low energy limit for the transmission coefficients calculations in the high-pressure limit.

In the high-pressure limit, it is likely that Complex-1 becomes stabilized and equilibrated, thus inducing the above described tunneling driven mechanism at very low temperatures. However, the following question arises: Is Complex-1 stabilized and equilibrated at lower pressures to an extent that the tunneling driven mechanism may play a role at very low temperatures? To address this question, we have calculated

the association rate constants $k_{ass}^{E,J-\mu VT}$ as funcion of pressure as well, and used these rate constants within the framework of the CUS theory (Eq. (22)) in order to estimate the total rate constant at low pressuress too.

Complex-1 can be stabilized by intermolecular collisions; lowering pressure tends to lower $k_{ass}^{E,J-\mu VT}$ (k_{stab} as defined in Eq. (10)) as these collisions become a rare event. This behaviour is shown in Figure 8, where it can be seen that this effect is especially important at high temperatures.

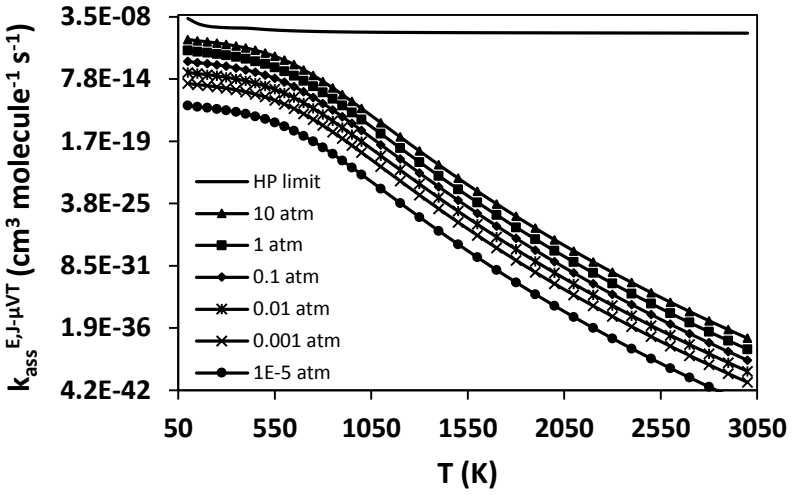

Figure 8. Plots of $k_{ass}^{E,J-\mu VT}$ (cm^3 molecule^{-1} s^{-1}), calculated at the M06-2X/6-311++G(2df,2pd) level, as function of temperature and pressure. HP stands for high-pressure.

The total k^{CUS} rate constant, calculated by Eq. (22), is also affected by the pressure dependence shown by the $k_{ass}^{E,J-\mu VT}$ rate constants. However, the final value of k^{CUS} is the result of the competition between the pressure effects when it comes to stabilize Complex-1, and the tunneling effect through the barrier separating that complex and the final products, that is, the $k_{ass}^{E,J-\mu VT}(P,T)$ and $k_{MS-T(C),f}^{CVT/SCT^*}(T)$ contributions to Eq. (22), respectively. Both contributions were considered to calculate $k^{CUS}(P,T)$, whose values are represented in Figure 9 at differents pressures between the high-pressure limit ($k_{MS-T(C),f}^{CVT/SCT^*}$ values in Table 3 and Figure 7) and a lower-pressure limit set to $1{\cdot}10^{-10}$ atm.

At high temperatures, when the tunneling effect contribution is negligible, the trend of k^{CUS} is governed by pressure effects; this is the reason for the observed decline as temperature increases, which is the result of the decrease of $k_{ass}^{E,J-\mu VT}$ as pressure is lowered. At low temperatures tunneling effect takes over and pressure effects are cancelled out, resulting in an increase in the values of k^{CUS}. In the limit of low pressure

($1 \cdot 10^{-10}$ atm), pressure effects are so pronounced that the increment in the value of k^{CUS} at low temperatures as consequence of tunneling is not observed. Therefore, Figure 9 shows how tunneling and pressure effects compete to determine the final value of k^{CUS}.

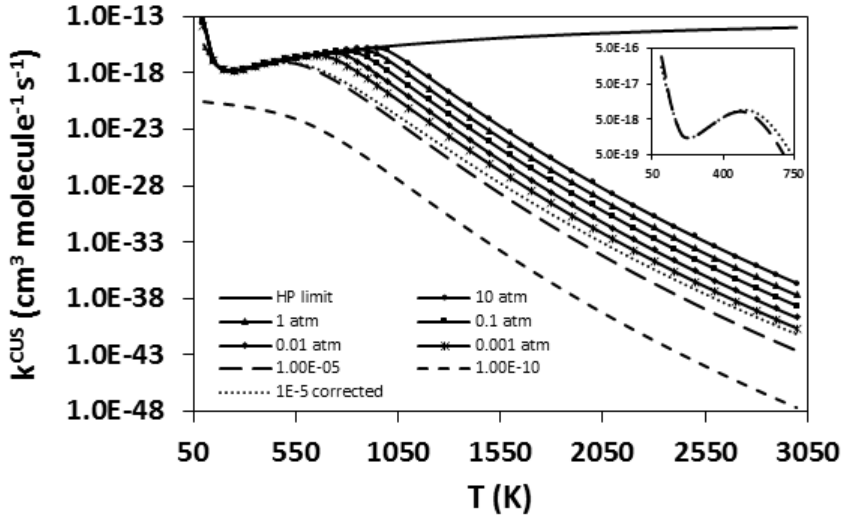

Figure 9. Plots of k^{CUS} (cm^3 molecule^{-1} s^{-1}), calculated at the M06-2X/6-311++G(2df,2pd) level using Eq. (22) with the $k_{ass}^{E,J-\mu VT}(P,T)$ and $k_{MS-T(C),f}^{CVT/SCT^*}(T)$ rate constants, as function of temperature and pressure. HP stands for high-pressure. The inset figure shows the values of k^{CUS} only at $1 \cdot 10^{-5}$ atm and temperatures between 50 and 750 K. The data labelled as "1E-5 corrected" (dotted line, $1 \cdot 10^{-5}$ atm) were obtained with a temperature-dependent $\langle \Delta E \rangle_{down}$ parameter by using Eq. (23).

Since $\langle \Delta E \rangle_{down}$ may have a marked temperature dependence, a sensitivity test on this parameter was performed to check how it affects the calculated rate constants. In our calculations, the value of $\langle \Delta E \rangle_{down}$ was 400 cm^{-1} for the reasons explained in Section 2.3. Our calculations were also carried out using the following temperature-dependent relation for $\langle \Delta E \rangle_{down}$

$$\langle \Delta E \rangle_{down} = \Theta \left(\frac{T}{300} \right)^{0.85} \quad (23)$$

where $\Theta = 300$ cm^{-1}. Eq. (23) yields values of $\langle \Delta E \rangle_{down}$ that varies from 117.9 cm^{-1} at 100 K to 2123.8 cm^{-1} at 3000 K, and the resulting rate constants are also represented in Figure 9 at $1 \cdot 10^{-5}$ atm (dotted line). At low temperatures, the enhancement of the reactivity is still present, and the new definition of $\langle \Delta E \rangle_{down}$ does not significantly affect the results. For instance, at 100 K and $1 \cdot 10^{-5}$ atm the values of k^{CUS} with values of $\langle \Delta E \rangle_{down}$ of 400 cm^{-1} and 117.9 cm^{-1} (according to Eq. (23)) are, respectively, $3.04 \cdot 10^{-16}$ and $1.52 \cdot 10^{-16}$ cm^3 molecule^{-1} s^{-1}.

It should be noted that the decline predicted by the SS-QRRK calculations at low pressures when temperature rises above 700 K is overestimated, and results from the large value of the thermal fraction of unimolecular states above the threshold energy, F_E, which is an estimation of the density of states $\rho(E)$,[42] defined by Troe[43] as

$$F_E \simeq \sum_{i=0}^{s-1} \frac{(s-1)!}{(s-1-i)!} \left[\frac{k_b T}{E_o + \alpha(E_o) E_{ZPE}}\right]^i \tag{24}$$

where $\alpha(E_o)$ is a correction factor[43] and E_{ZPE} is the ZPE of the activated complex. F_E is used to determine the collision efficiency β_c, which is used to calculate the collisional deactivation rate constant k_c (Eq. (11)), and is defined as[44]

$$\beta_c = \left(\frac{\langle \Delta E \rangle_{down}}{\langle \Delta E \rangle_{down} + F_E k_b T}\right)^2 \tag{25}$$

Troe pointed out that F_E adopts values near 1 for moderately sized molecules at not too high temperatures (≈ 1000 K), and adopts values much larger than 1 for molecules with more than around eight atoms in that high temperature regime.[43] A decrease in the values of the collision efficiency when large F_E values are obtained at high temperatures, and therefore a decrease in the collisional deactivation rate constant too, is physically correct; however, the description obtained by Eq. (25) might be unrealistic for large systems and temperatures above 1000 K,[44] yielding too low values of β_c and therefore understimating k_{stab} ($k_{ass}^{E,J-\mu VT}$ in our formulation) and k^{CUS} at high temperatures, as shown in Figures 8 and 9.

A better description of β_c which would help to correct the observed overestimated decrease in the rate constants would be that proposed by Gilbert *et al*.,[44]

$$\beta_c' = \left(\frac{\langle \Delta E \rangle_{down}}{\langle \Delta E \rangle_{down} + F_E k_b T}\right)^2 \frac{1}{\Delta} \tag{26}$$

in which a correction factor Δ^{-1} is used in order to obtain more realistic values. This correction factor can be calculated if the functions F_E and $\rho(E)$ are known. In this work, we did not attempt to calculate Δ^{-1} to correct β_c. However, we show that under the strong-collision assumption, which assumes that every collision of the energized complex leads to de-energization ($\beta_c = 1$), Eq. (11) becomes

$$k_c(T) = Z \tag{27}$$

Therefore, at very low pressures the term $k_c[M]$ in the denominator of Eq. (10) can be neglected, and the pressure dependent rate constants can be redefined as

$$k_{stab} = k_{ass}^{E,J-\mu VT} \sum_{E_o}^{+\infty} \frac{Z[M] f(E)}{k_{-1}^{QRRK}(E)} \tag{28}$$

We used Eq. (28) and corrected k_{stab} at 0.01 and 0.001 atm, obtaining corrected k^{CUS} values as well. These corrected k^{CUS} rate constants are plotted in Figure 10 together with those calculated using the former definition of k_{stab} (non-corrected, Figure 9), showing that the decreasing trend beyond 700 K is significantly mitigated. They are also tabulated in Table 4. The correction of that trend is practically complete due to the use of the strong-collision assumption (negligible differences can be observed at very high temperatures in the inset figure though). Values of β_c lower than 1 would lead to a partial correction and migth be more realistic, but would require the determination of the correction factor Δ^{-1}, which is beyond the scope of the present work.

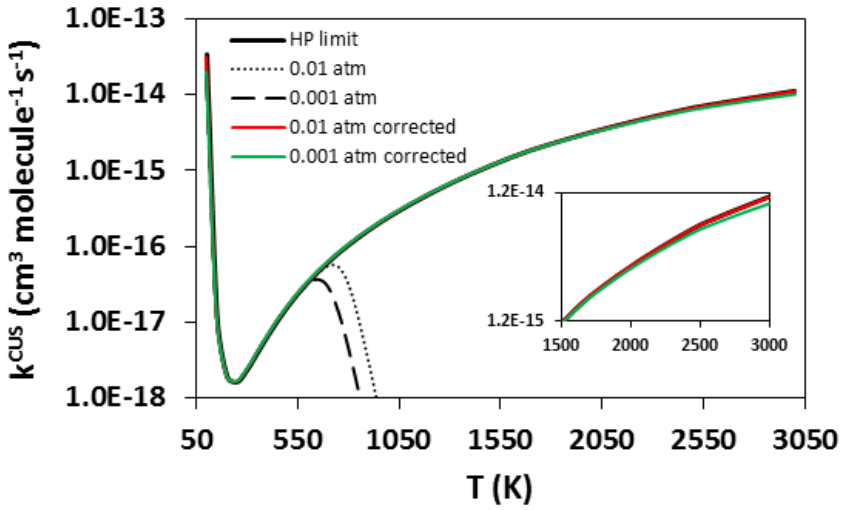

Figure 10. Plots of the corrected and non-corrected k^{CUS} values (cm^3 molecule^{-1} s^{-1}), calculated at the M06-2X/6-311++G(2df,2pd) level using Eq. (22) with the $k_{ass}^{E,J-\mu VT}(P,T)$ and $k_{MS-T(C),f}^{CVT/SCT^*}(T)$ rate constants, as function of temperature and pressure. High pressure values (HP) are also shown.

Table 4. Thermal corrected rate constants k^{CUS} (cm^3 molecule^{-1} s^{-1}) at the M06-2X/6-311++G(2df,2pd) level at 0.01 and 0.001 atm.

T (K)	k^{CUS}(0.001 atm)	k^{CUS}(0.01 atm)
100	$1.94\cdot10^{-14}$	$3.16\cdot10^{-14}$
150	$1.21\cdot10^{-17}$	$1.21\cdot10^{-17}$
200	$1.90\cdot10^{-18}$	$1.90\cdot10^{-18}$
250	$1.64\cdot10^{-18}$	$1.64\cdot10^{-18}$
298	$2.35\cdot10^{-18}$	$2.35\cdot10^{-18}$
400	$6.61\cdot10^{-18}$	$6.61\cdot10^{-18}$

500	$1.63 \cdot 10^{-17}$	$1.63 \cdot 10^{-17}$
600	$3.41 \cdot 10^{-17}$	$3.41 \cdot 10^{-17}$
700	$6.27 \cdot 10^{-17}$	$6.27 \cdot 10^{-17}$
800	$1.05 \cdot 10^{-16}$	$1.05 \cdot 10^{-16}$
900	$1.65 \cdot 10^{-16}$	$1.66 \cdot 10^{-16}$
1000	$2.47 \cdot 10^{-16}$	$2.48 \cdot 10^{-16}$
1100	$3.55 \cdot 10^{-16}$	$3.57 \cdot 10^{-16}$
1200	$4.94 \cdot 10^{-16}$	$4.97 \cdot 10^{-16}$
1400	$8.84 \cdot 10^{-16}$	$8.95 \cdot 10^{-16}$
1600	$1.46 \cdot 10^{-15}$	$1.49 \cdot 10^{-15}$
1800	$2.20 \cdot 10^{-15}$	$2.26 \cdot 10^{-15}$
2000	$3.09 \cdot 10^{-15}$	$3.21 \cdot 10^{-15}$
2300	$4.82 \cdot 10^{-15}$	$5.11 \cdot 10^{-15}$
2500	$6.24 \cdot 10^{-15}$	$6.72 \cdot 10^{-15}$
2800	$8.31 \cdot 10^{-15}$	$9.15 \cdot 10^{-15}$
3000	$9.90 \cdot 10^{-15}$	$1.11 \cdot 10^{-14}$

The net result of the observed trade-off between pressure and tunneling effects is an enhancement of the i-C_3H_5OH + HO_2 → CH_3COCH_3 + HO_2 process at ultracold temperatures and even at low pressures (above $1 \cdot 10^{-5}$ atm), leaning the keto−enol tautomerism even more to the keto form. This tunneling mediated mechanism has been suggested as a precursor and processor of complex organic molecules in interstellar clouds, in which the ultracold temperatures hinder the reactivity. This is the case of the reaction between methanol and the hydroxyl radical, which has been proven, theoretically and experimentally, as a sink of this alcohol in that medium. Theoretically, a pronounced tunneling effect associated to the presence of a pre-reactive complex was found for this reaction.[45,46] For instance, Gao *et al*.[46] calculated a value of $3.06 \cdot 10^{-13}$ cm^3 $molecule^{-1}$ s^{-1} at 100 K and $1.6 \cdot 10^{-3}$ atm, which is around one order of magnitude larger than the value we calculated at the same temperature and $1.0 \cdot 10^{-3}$ atm; this suggests that the reaction studied in this work may be also competitive under these conditions of low temperature and pressures. Our work is also helpful to understand and model the formation and consumption of complex organic molecules with several heavy atoms in the interstellar medium. Our rate constants and findings at very low temperatures and pressures can be also used as analogies to model similar keto−enol tautomerisms involving other enols that may be present in these environments.

Not only the tunneling effect, but also the large values of $k_{ass}^{E,J-\mu VT}$ obtained in our calculations contributed to mitigate the negative effect that pressure has on k^{CUS}, and therefore to the observed tunneling

mediated mechanism even in the low pressure regime; $k_{ass}^{E,J-\mu VT}$ is still very large even at low temperatures and low pressures, with values of, for example, $3.1 \cdot 10^{-14}$ cm^3 molecule^{-1} s^{-1} at 100 K and 0.001 atm (Figure 8). However, some possible sources of error in our calculations should be discussed. The level of theory used to analyze the effect of the intermediate Complex-1, M06-2X/6-311++G(2df,2pd), was chosen as a compromise between accuracy and computational cost. In our analysis of the effect of the intermediate complex, the VRC-*E,J*-μVT calculations represent a bottleneck, and thus a higher level of theory is not feasible. Nevertheless, its predictions are in good agreement to those at the higher level CCSD(T)/aug-cc-pVTZ//M06-2X/cc-pVTZ, as was explained in Section 3.2. The ZPE-corrected energy of Complex-1, with respect to that of the reactants, predicted by the lower level is 0.8 kcal mol^{-1} lower than that of the higher level. This suggests that the values of $k_{ass}^{E,J-\mu VT}$ at the M06-2X/6-311++G(2df,2pd) level might be slightly overestimated, and therefore, the increase of k^{CUS} observed at very low temperatures might be less pronounced when a more accurate level is used. Tunneling through the barrier separating Complex-1 and Complex-2 should be similar with both levels of theory though, as these barriers are 14.4 and 13.7 kcal mol^{-1} with the higher and lower level, respectively; however, some differences may also arise.

4. CONCLUSIONS

In this work, a theoretical kinetic study of the HO_2-catalyzed tautomerism converting propen-2-ol into acetone, i-C_3H_5OH + HO_2 ⇔ CH_3COCH_3 + HO_2, has been carried out by running CCSD(T)/aug-cc-pVTZ//M06-2X/cc-pVTZ *ab initio* calculations and using the multi-structural torsional variational transition state theory with tunneling corrections, the variable reaction coordinate theory, and the system-specific quantum Rice-Ramsperger-Kassel theory. We have demonstrated the pronounced catalytic effect of the HO_2 radical, which promotes a double hydrogen atom transfer reaction and lowers the adiabatic barrier from 54.0 kcal mol^{-1} in the non-catalyzed process to 7.2 kcal mol^{-1}. A wide temperature range, 100–3000 K, and pressures as low as $1 \cdot 10^{-5}$ atm have been covered in our kinetic study; to the best of our knowledge, no rate constants have been reported for the studied reaction yet. Therefore, our calculated rate constants are useful to avoid the use of analogue reactions when it comes to model combustion, atmospheric, and interstellar processes in which the studied tautomerism could play a role.

An interesting feature of the PES of the studied reaction is the formation of an intermediate complex, Complex-1, on the entry channel as a result of a highly stabilizing OH···π hydrogen bond between the HO_2 radical and the double bond of the i-C_3H_5OH molecule. The rate constants for the formation of Complex-1 were calculated with the variable reaction coordinate theory, which allowed us to apply the canonical unified statistical model to determine the effect of this intermediate on the calculated forward rate constants. At temperatures between 250 K and 3000 K, covering temperatures of interest in atmospheric and

combustion processes, Complex-1 has no effect on the kinetics, and the reaction i-C_3H_5OH + HO_2 ⇔ CH_3COCH_3 + HO_2 takes place in a single-step mechanism.

We have updated a former kinetic model for the pyrolysis and combustion of butanol isomers with our calculated rate constants in order to assess the importance of the studied reaction in the combustion of 2-butanol, s-C_4H_9OH. In the former model, this reaction is included by means of an analogy to the HO_2-catalyzed tautomerism that converts vinyl alcohol into acetaldehyde. Then, we compared the performance of the two models, former and updated, in the combustion of s-C_4H_9OH by running closed batch and perfectly stirred reactor simulations in CHEMKIN. Despite the catalytic effect of the HO_2 radical, the HO_2-catalyzed reaction turned out to be unimportant in the consumption of i-C_3H_5OH and production of CH_3COCH_3 during the combustion of the fuel, which may be due to the low concentration of HO_2. Instead, the tautomerism converting i-C_3H_5OH into CH_3COCH_3 is governed by the reactions i-C_3H_5OH ⇔ CH_3COCH_3 and i-C_3H_5OH + HCOOH ⇔ CH_3COCH_3 + HCOOH. The unimolecular tautomerism consumes i-C_3H_5OH since the very beginning as there is no need of a second partner. The HCOOH-catalyzed reaction is much more favorable due to the more efficient catalytic effect of HCOOH, which is present in a lower concentration than HO_2. However, the rate constants for the reaction i-C_3H_5OH + HCOOH ⇔ CH_3COCH_3 + HCOOH are also included in current models by means of an analogy to the reaction of vinyl alcohol, and no calculated rate constants are available. Therefore, these findings might be subjected to a proper description of the HCOOH-catalyzed tautomerism.

At ultracold temperatures, of interest in the chemistry of interstellar environments such as interstellar clouds, the pre-reactive complex can play a role in the kinetics of the studied tautomerism as it can be stabilized even at very low presures. Under this scenario, the canonical unified statistical model predicts a significant enhancement of the reactivity at temperatures within the 100–250 K range as the result of a tunneling driven process, suggesting a step-wise mechanism i-C_3H_5OH + HO_2 ⇔ Complex-1 → CH_3COCH_3 + HO_2. Our calculations at ultracold temperatures and low pressures help to understand and model the fate of complex organic molecules, such as i-C_3H_5OH and CH_3COCH_3, in the interstellar medium. In addition, given the abundance of different alcohols in interstellar clouds, other enols that can undergo a similar keto−enol tautomerism could be also modelled with the rate constants reported in this work as an analogy.

SUPPORTING INFORMATION

Electronic supplementary information available with details regarding the transmission coefficients calculations. The updated kinetic model is also provided as supporting information.

AUTHOR INFORMATION

Corresponding author

(M. M.-P.) E-mail: manuel.mongepalacios@kaust.edu.sa

ORCID

M. Monge-Palacios: : 0000-0003-1199-5026

E. Grajales- González: 0000-0002-2317-0884

S. Mani Sarathy: 0000-0002-3975-6206

Notes

The authors declare no cometing financial interest.

ACKNOWLEDGMENTS

The research reported in this publication was supported by funding from King Abdullah University of Science and Technology (KAUST), Office of Sponsored Research (OSR) under Award No. OSR-2016-CRG5-3022. We thank the resources of the Supercomputing Laboratory at KAUST. We are grateful to María Cecilia Alvarado Bernáldez for her assistance in designing and elaborating the TOC graphic.

REFERENCES

(1) S. Mani Sarathy, P. Oßwald, N. Hansen and K. Kohse-Höinghaus, Alcohol Combustion Chemistry, *Prog. Energy Combust. Sci*. 2014, **44**, 40-102.

(2) C. A. Taatjes, N. Hansen, A. Mcllroy, J. A. Miller, J. P. Senosiain, S. J. Klippenstein, F. Qi, L. Sheng, Y. Zhang, T. A. Cool et al., Enols Are Common Intermediates in Hydrocarbon Oxidation, *Science* 2005, **308**, 1887-1889.

(3) S. Mani Sarathy, S. Vranckx, K. Yasunaga, M. Mehl, P. Oßwald, W. K. Metcalfe, C. K. Westbrook, W. J. Pitz, K. Kohse-Höinghaus, R. X. Fernandes and H. J. Curran, A Comprhenhensive Chemical Kinetic Combustion Model for the Four Butanol Isomers, *Combustion and Flame* 2012,**159**, 2028-2055.

(4) E. Grajales-González, M. Monge-Palacios and S. Mani Sarathy, Theoretical Kinetic Study of the Unimolecular Keto−Enol Tautomerism Propen-2-ol ↔ Acetone. Pressure Effects and Implications in the Pyrolysis of tert- and 2-Butanol, *J. Phys. Chem. A*, 2018, **122**, 3547-3555.

(5) G. da Silva, C.-H. Kim and J. W. Bozzelli, Thermodynamic Properties (Enthalpy, Bond Energy, Entropy, and Heat Capactiy) and Internal Rotor Potentials of Vinyl Alcohol, Methyl Vinyl Ether, and Their Corresponding Radicals, *J. Phys. Chem. A* 2006, **110**, 7925-7934.

(6) K. Yasunaga, T. Mikajiri, S. M. Sarathy, T. Koike, F. Gillespie, T. Nagy, J. M. Simmie and H. J. Curran, A Shock Tube and Chemical Kinetic Modeling Study of the Pyrolysis and Oxidation of Butanols, *Combust. Combust. Flame* 2012, **159**, 2009-2027.

(7) G. da Silva and J. W. Bozzelli, Role of the α-hydroxyethylperoxy radical in the reactions of acetaldehyde and vinyl alcohol with HO2, *Chem. Phys. Lett*. 2009, **483**, 25-29.

(8) B. E. Turner and A. J. Apponi, Microwave Detection of Interstellar Vinyl Alcohol, CH2=CHOH, *Astrophysical Journal*, 2001, **561**, L207-L210.

(9) L. Harvey-Smith and R. J. Cohen, Discovery of Large-Scale Methanol and Hydroxyl Maser Filaments in W3(OH), *Mon. Not. R. Astrom. Soc*. 2006, **371**, 1550-1558.

(10) F. Combes, M. Gerin, A. Wootten, G. Wlodarczak, F. Clausset and P. J. Encrenaz, Acetone in Interstellar Space, *Astron. Astrophys*. 1987, **180**, L13-L16.

(11) D. N. Friedel, L. E. Snyder, A. J. Remijan and B. E. Turner, Detection of Interstellar Acetone toward the Orion-KL Hot Core, *Astrophys. J. Lett*. 2005, **632**, L95-L98.

(12) M. A. Requena-Torres, J. Martin-Pintado, S. Martin and M. R. Morris, The Galactic Center: The Largest Oxygen-bearing Organic Molecule Repository, *Astrophysical Journal* 2008, **672**, 352-360.

(13) J. M. Hollis, P. R. Jewell, F. J. Lovas, A. Remijan and H. Mollendal, Green Bank Telescope Detection of New Interstellar Aldehydes: Propenal and Propanal, *Astrophysical Journal* 2004, **610**, L21-L24.

(14) A. Karton and D. Talbi, Pinning the Most Stable $H_xC_yO_z$ Isomers in Space by Means of High-level Theoretical Procedures, *Chem. Phys.* 2014, **436-437**, 22-28.

(15) G. da Silva, Carboxylic Acid Catalyzed keto–enol Tautomerizations in the Gas Phase, *Angew. Chem. Int*. Ed. 2010, **49**, 7523-7525.

(16) D. G. Truhlar, A. D. Isaacson and B. C. Garrett, Theory of Chemical Reaction Dynamics, M. Baer, Ed., CRC Press: Boca Raton 1985, **4**, 65.

(17) M. J. Frisch, G. W. Trucks, H. B. Schlegel, G. E. Scuseria, M. A. Robb, J. R. Cheeseman, G. Scalmani, V. Barone, B. Mennucci, G. A. Petersson et al., Gaussian 09, Gaussian, Inc, Wallingford, CT (2010).

(18) Y. Zhao and D. G. Truhlar, The M06 Suite of Density Functionals for Main Group Thermochemistry, Thermochemical Kinetics, Noncovalent Interactions, Excited States, and Transition Elements: Two New Functionals and Systematic Testing of Four M06-class Functionals and 12 Other Functionals, *Theor. Chem. Acc*. 2008, **120**, 215-241.

(19) T. H. Dunning Jr., Gaussian Basis Sets for Use in Correlated Molecular Calculations. I. The Atoms Boron Through Neon and Hydrogen, *J. Chem. Phys*. 1989, **90**, 1007-1023.
(20) R. J. Bartlett, Coupled-Cluster Approach to Molecular Structure and Spectra: a Step toward Predictive Quantum Chemistry, *J. Phys. Chem*. 1989, **93**, 1697-1708.
(21) J. Zheng, S. Zhang, J. C. Corchado, R. Meana-Pañeda, Y. Y. Chuang, E. L. Coitiño, B. A. Ellingson and D. G. Truhlar, GAUSSRATE 2016, University of Minnesota: Minneapolis (2016).
(22) M. Page and J. W. McIver, On Evaluating the Reaction Path Hamiltonian, *J. Chem. Phys.* 1988, **88**, 922-935.
(23) J. Zheng, T. Yu, E. Papajak, I. M. Alecu, S. L. Mielke and D. G. Truhlar, Practical Methods for Including Torsional Anharmonicity in Thermochemical Calculations on Complex Molecules: The Internal-coordinate Multi-structural Approximation, *Phys. Chem. Chem. Phys*. 2011, **13**, 10885-10907.
(24) J. Zheng and D. G. Truhlar, Quantum Thermochemistry: Multistructural Method with Torsional Anharmonicity Based on a Coupled Torsional Potential, *J. Chem. Theory Comput*. 2013, **9** 1356-1367.
(25) J. Zheng, J. L. Bao, R. Meana-Pañeda, S. Zhang, B. J. Lynch, J. C. Corchado, Y-Y. Chuang, P. L. Fast, W-P. Hu, Y-P. Liu et al., POLYRATE-version 2016-2A, Univeristy of Minnesota: Minneapolis (2016).
(26) J. Zheng, S. L. Mielke, K. L. Clarkson, R. Meana-Pañeda and D. G. Truhlar, MSTor, version 2013, University of Minnesota: Minneapolis (2013).
(27) NIST Computational Chemistry Comparison and Benchmark Database, NIST Standard Reference Database Number 101 2016, Ed. Russell D. Johnson III, available at <http://cccbdb.nist.gov/>.
(28) Y. Georgievskii and S. J. Klippenstein, Variable Reaction Coordinate Transition State Theory: Analytic Results and Application to the C2H3+H→C2H4 reaction, *J. Chem. Phys*. 2003, **118**, 5442-5455.
(29) Y. Georgievskii and S. J. Klippenstein, Transition State Theory for Multichannel Addition Reactions: Multifaceted Dividing Surfaces, *J. Phys. Chem. A* 2003, **107**, 9776-9781.
(30) J. L. Bao and D. G. Truhlar, SS-QRRK: A Program for System-Specific Quantum Rice-Ramsperger-Kassel Theory, version 2016-2A, Univeristy of Minnesota: Minneapolis (2017).
(31) R. S. Zhu and M. C. Lin, Ab Initio Studies of ClOX Reactions: Prediction of the Rate Constants of ClO+NO for the Forward and Reverse Processes, Chem. Phys. Chem. 2004, **5**, 1864-1870.
(32) B. Laszlo, S. Dobe, T. Berces and F. Marta, Twelfth International Symposium on Gas Kinetics, 1992.
(33) Reactor Design, CHEMKIN-PRO18.1: San Diego, 2017.
(34) T. J. Lee and P. R. Taylor, A Diagnostic for Determining the Quality of Single-Reference Electron Correlation Methods, *Int. J. Quantum Chem., Quantum Chem. Symp.* 1989, **S23**, 1999.

(35) P. Ottiger, C. Pfaffen, R. Leist and S. Leutwyler, Strong N-H···π Hydrogen Bonding in Amide-Benzene Interactions, *J. Phys. Chem. B* 2009, **113**, 2937-2943.

(36) M. Nishio, Y. Umezawa, J. Fantini, M. S. Weiss and P. Chakrabarti, CH–π Hydrogen Bonds in Biological Macromolecules, *Phys. Chem. Chem. Phys*. 2014, **16**, 12648-12683.

(37) D. P. Mukhopadhyay, S. Biswas, A. Chattopadhyay and T. Chakraborty, Conformational Preference Determined by C−H···π Interaction of an O−H···O Hydrogen-Bonded Binary Complex of *p*-Fluorophenol with 2,5-Dihydrofuran: A Laser-Induced Fluorescence Spectroscopy Study, *J. Phys. Chem. A* 2018, **122**, 3787-3797.

(38) F. Holland, A. Hofzumahaus, J. Schafer, A. Kraus and H.-W. Patz, Measurements of OH and HO2 Radical Concentrations and Photolysis Frequencies during BERLIOZ, *J. Gophys. Res.* 2003, **108**, 1-21.

(39) M. Monge-Palacios, M. P. Rissanen, Z. Wang and S. M. Sarathy, Theoretical Kinetic Study of the Formic Acid Catalyzed Criegee Intermediate Isomerization: Multistructural Anharmonicity and Atmospheric Implications, *Phys. Chem. Chem. Phys*. 2018, **20**, 10806-10814.

(40) M. Monge-Palacios and S. Mani Sarathy, *Ab initio* and Transition State Theory Study of the *Ab Initio* and Transition State Theory Study of the OH + $HO_2 \rightarrow H_2O + O_2(^3\Sigma_g^-)/O_2(^1\Delta_g)$ Reactions: Yield and Role of $O_2(^1\Delta_g)$ in H_2O_2 Decomposition and in Combustion of H_2, *Phys. Chem. Chem. Phys.* 2018, **20**, 4478-4489.

(41) M. Monge-Palacios, C. Rangel, J. C. Corchado and J. Espinosa-García, Analytical Potential Energy Surface for the Reaction with Intermediate Complexes $NH_3 + Cl \rightarrow NH_2 + HCl$: Application to the Kinetics Study, *Int. J. Quantum Chem*. 2012, **112**, 1887-1903.

(42) J. Troe, Theory of Thermal Unimolecular Reactions at Low Pressures. I. Solutions of the Master Equation, *J. Chem. Phys.* 1977, **66**, 4745-4757.

(43) J. Troe, Predictive Possibilities of Unimolecular Rate Theory, *J. Phys. Chem.* 1979, **83**, 114-126.

(44) R. G. Gilbert, K. Luther and J. Troe, Theory of Thermal Unimolecular Reactions in the Fall-off Range. II. Weak Collision Rate Constants, *Berichte Der Bunsengesellschaft Für Phys. Chemie* 1983, **87**, 169-177.

(45) R. J. Shannon, M. A. Blitz, A. Goddard and D. E. Heard, Accelerated Chemistry in the Reaction between the Hydroxyl Radical and Methanol at Interstellar Temperatures Facilitated by Tunneling, *Nat. Chem*. 2013, **5**, 745-749.

(46) L. G. Gao, J. Zheng, A. Fernandez-Ramos, D. G. Truhlar and X. Xu, Kinetics of the Methanol Reaction with OH at Interstellar, Atmospheric, and Combustion Temperatures, *J. Am. Chem. Soc*. 2018, **140**, 2906-2918.

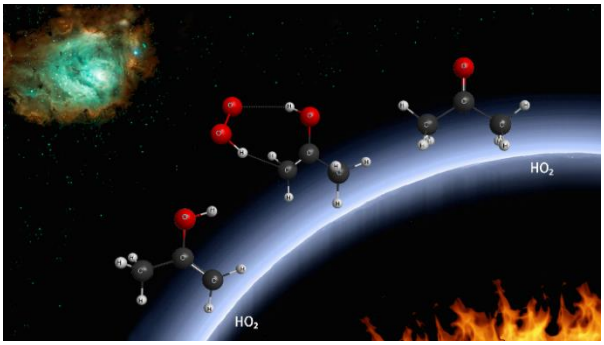

TOC Graphic